Journal of Catalysis **190,** 14–21 (2000)
doi:10.1006/jcat.1999.2722, available online at http://www.idealibrary.com on IDEAL®

CH_3 and CH_2 Oxidation Reactions on MoO_3(100): Analysis of the Electronic Structure

B. Irigoyen, A. Juan,[1] and N. Castellani

Departamento de Física, Universidad Nacional del Sur, Avda. Alem 1253, 8000 Bahía Blanca, Argentina

Received March 3, 1999; revised October 4, 1999; accepted October 13, 1999

The oxidation reactions of CH_3 and CH_2 fragments on MoO_3(100) were studied following the changes in the electronic structure and the bonding character of the bonds between the adsorbed fragments and the MoO_3 surface atoms. The adsorption energy for these fragments was computed using a methodology based on the atomic superposition and electron delocalization molecular orbital theory. The electronic structure was analyzed by the local density of states concept. A detailed picture of the bonding between fragments and the surface is given by examining the overlap population. In the homolytic mechanism each C–H bond breakage occurs before the corresponding hydrocarbon fragment reaches the energy barrier and the O–H is formed after surmounting this barrier. A strong C–O chemical bond is established as a consequence of the last H abstraction. On the other hand, in the heterolytic mechanism the C–H breaking is accompanied by a temporarily weakening of a second C–H bond and the formation of an increasingly strong C–Mo bond. In the last H abstraction of methane decomposition the C–H bond is broken only in the final step. While on the layer of MoO_3 exposing mainly O atoms, the interactions between the CH_3 or the CH_2 fragment and the surface O atom are negligible; on the layer of MoO_3 exposing Mo atoms, the molecular orbitals of these fragments show an important hybridization due to the significant C–Mo chemical interaction.

Key Words: **methyl adsorption; methylene adsorption; molybdenum oxide; ASED-MO; LDOS; oxidation catalysts.**

1. INTRODUCTION

Considerable efforts have recently been made to understand the partial oxidation of methane to produce chemicals of commercial interest using oxide-based catalysts (1–6). The generally accepted idea is that the first step in activating methane is the abstraction of a hydrogen atom to give methyl fragments adsorbed on the oxide surface. Nevertheless, the mechanism of the C–H bond breaking and the nature and the role played by the active oxygen species are the object of extensive speculations.

Two main reaction mechanisms were proposed. The most cited is named as the heterolytic (7, 8) and the other constitutes the homolytic mechanism (9). In the first one, a H^+ and a methyl anion (CH_3^-) are produced, while in the second a reduced oxygen species of the surface could be responsible for the abstraction, resulting in the production of two rather electroneutral species.

Molybdenum trioxide is known as an active and selective catalyst for the partial oxidation of alcohols and hydrocarbons (10–12). In addition, MoO_3-based catalysts are widely studied for methane oxidation (13–18).

During recent years a number of papers describing reactions for synthesizing oxygenated products from CO and H_2 and for the reduction of NO_x appeared, where catalysts based on metals modified by Mo or molybdenum oxides were used. These studies showed that the incorporation of Mo in the form of MoO_3 to Pd or Pt catalysts significantly improved not only the NO conversion under reducing conditions, with minimal NH_3 formation, but also the NO reactivity under slightly oxidizing conditions (19, 20). Experimental studies performed in our laboratory for methane combustion using Pd–MoO_3/Al_2O_3 indicated the promotional effect of MoO_3 (21). Extensive revisions on oxidation catalysts were published (22). Particularly, the role of molybdenum oxide surfaces on methane and methanol oxidation was described in (23).

Focusing on the theoretical approaches, the extended Hückel (E/H) method was employed by several authors to study the interactions of alcohol and hydrocarbon molecules with metal oxide surfaces (24–26). This formalism was used by Sambeth *et al.* to explain the catalytic oxidation of methanol on V_2O_5 (24). The chemisorption of methanol on various faces of MoO_3 was studied by Rahmouni and Barbier (25). The CH_3OH dehydrogenation proceeding on a Keggin structure, composed of V–O–V oxygen bridges and V=O terminal groups, was considered by Weber (26). According to this author, the oxidative dehydrogenation process implies the interaction between an antibonding orbital directed along a C–H bond of the CH_3OH and the HOMO of the cluster, facilitating the transfer of hydrogen toward a metal cation center (M^+). During this transfer the H–*M* interaction is bonding while the H–O interaction with the adjacent oxygen atom is antibonding. The fact that the

[1] To whom correspondence should be addressed. E-mail: cajuan@criba.edu.ar. Fax: 54-291-4595142.

0021-9517/00 $35.00

addition of electrons (by reduction) to the V–O–V chain weakens the O–V bonds, resulting in a more reactive oxygen atom during the dehydrogenation oxidative process, was also indicated by this author.

Important conclusions concerning the dissociative chemisorption of methane on MoO_3 surfaces in the presence of O^- species were drawn by the calculations of Mehandru *et al.* (27). The results obtained using the atomic superposition and electron delocalization molecular orbital theory (ASED-MO) on a $Mo_3O_{11}^{4-}$ cluster showed that O^- strongly activates the C–H bond in methane. The presence of O^- was explained in terms of a O $2p \rightarrow$ Mo $4d$ charge-transfer excitation by ultraviolet radiation. Heterolytic adsorption most likely occurs at edge sites and CH_3^- forms a donor bond to Mo^{6+} (27).

Recently, a theoretical study of the dehydrogenation and subsequent oxidation of methane at different catalytic sites of a MoO_3(100) surface was reported by our group (28). A semiempirical molecular orbital technique (ASED-MO) was employed for this purpose. From these calculations it was concluded that the heterolytic H abstraction is an energetically more favorable process compared with the homolytic one. The process is known to be endothermic. The purpose of the present paper, following our previous calculations, is to analyze the electronic structure mainly by examining overlap populations to give a more detailed picture of the bonding.

2. THEORETICAL METHODS

The interactions between the hydrocarbon fragments and the MoO_3 surface were performed using the ASED-MO (29–31) technique. This method is a modification of the traditional E-H theory (32). The atomic parameters used for the present work are the same as those in Ref. (28). Our calculations were performed using a bulk superimposable $Mo_{30}O_{107}^{34-}$ cluster. The excess electrons assigned to the cluster, causing it to formally bear a charge of -34, serve to assure that all oxygen anions have a -2 charge. This -34 charge does not affect the evaluation of the electronic Hamiltonian matrix elements under the standard EH calculations (29–32).

The adsorption energy was calculated as (28)

$$\Delta E_{\text{total}} = E_{\text{total}}(\text{ads. species/metal oxide}) - E_{\text{total}}(\text{species}) - E_{\text{total}}(\text{metal oxide}). \quad [1]$$

The electronic structure of the oxide and the different adsorbed species was analyzed in terms of the density of electronic states (DOS) and of the projected local density of electronic states (p-LDOS), respectively. The first is defined by

$$\text{DOS}(E) = \sum_i g(E - E_i), \quad [2]$$

where $g(E - E_i)$ is a gaussian convolution function centered on energy E_i corresponding to molecular orbital "i" of the MoO_3 cluster. The p-LDOS of molecular orbital α of the CH_n fragment, on the other hand, is defined as follows,

$$\text{p-LDOS}_\alpha(E) = \sum_i |\langle \alpha \mid i \rangle|^2 g(E - E_i), \quad [3]$$

where $|\langle \alpha \mid i \rangle|^2$ gives the projection of molecular orbital "i" of the $CH_n + MoO_3$ cluster system onto the molecular orbital α of the fragment. The integration of this variable up to the Fermi level constitutes the population of molecular orbital α.

Another useful concept is that of the overlap population, "OP" (a–b), between two atoms named as "a" and "b." In this case, the Mülliken population analysis was used (33, 34). This magnitude depends on the atomic coefficients of eigenvectors and the overlap interatomic integrals and it can be considered as a measure of bonding between the atoms.

3. RESULTS AND DISCUSSION

The overall oxidative dehydrogenation reactions of methane on MoO_3(100) were studied in a previous paper by performing the calculation of the adsorption energy corresponding to CH_4 and its various dehydrogenated compounds, during the overall $CH_3 \rightarrow CH_2 \rightarrow CH \rightarrow C$ process (28). The adsorption energy change versus the reaction coordinate curve for H abstraction has shown a series of hills and valleys (see Fig. 1). The activation energy for the first dehydrogenation is greater than those for the second and third H abstractions, implying that the methane activation is kinetically controlled only by the former of these processes. Once the first barrier is overcome, both CH_3 or CH_2 could be produced, with a different energetic cost in each case. Nevertheless, the next $CH_2 \rightarrow CH + H$ reaction is thermodynamically unfavorable, unless additional energy is provided. This observation suggests that MoO_3 would be a selective catalyst, capable of limiting subsequent methyl decomposition.

In the different homolytic or heterolytic mechanisms for the hydrogen abstraction from CH_4, the formation of several chemical bonds is established between one of the adsorbed species and another atom belonging to the oxide surface. In the homolytic case the carbon atom is finally bonded to an O atom of the "O" surface layer of MoO_3. On the other hand, in the heterolytic case the carbon atom bonds to a Mo atom of the "Mo" surface layer. In Fig. 1 (inserts) are shown the pathways for the second H abstraction from CH_3 over the "O" and "Mo" layers, respectively.

To obtain a more quantitative picture of the chemical interaction present between the adsorbed species and the oxide surface, the overlap population "OP" for the C–H, C–O, C–Mo, and O–H bonds was calculated. The results

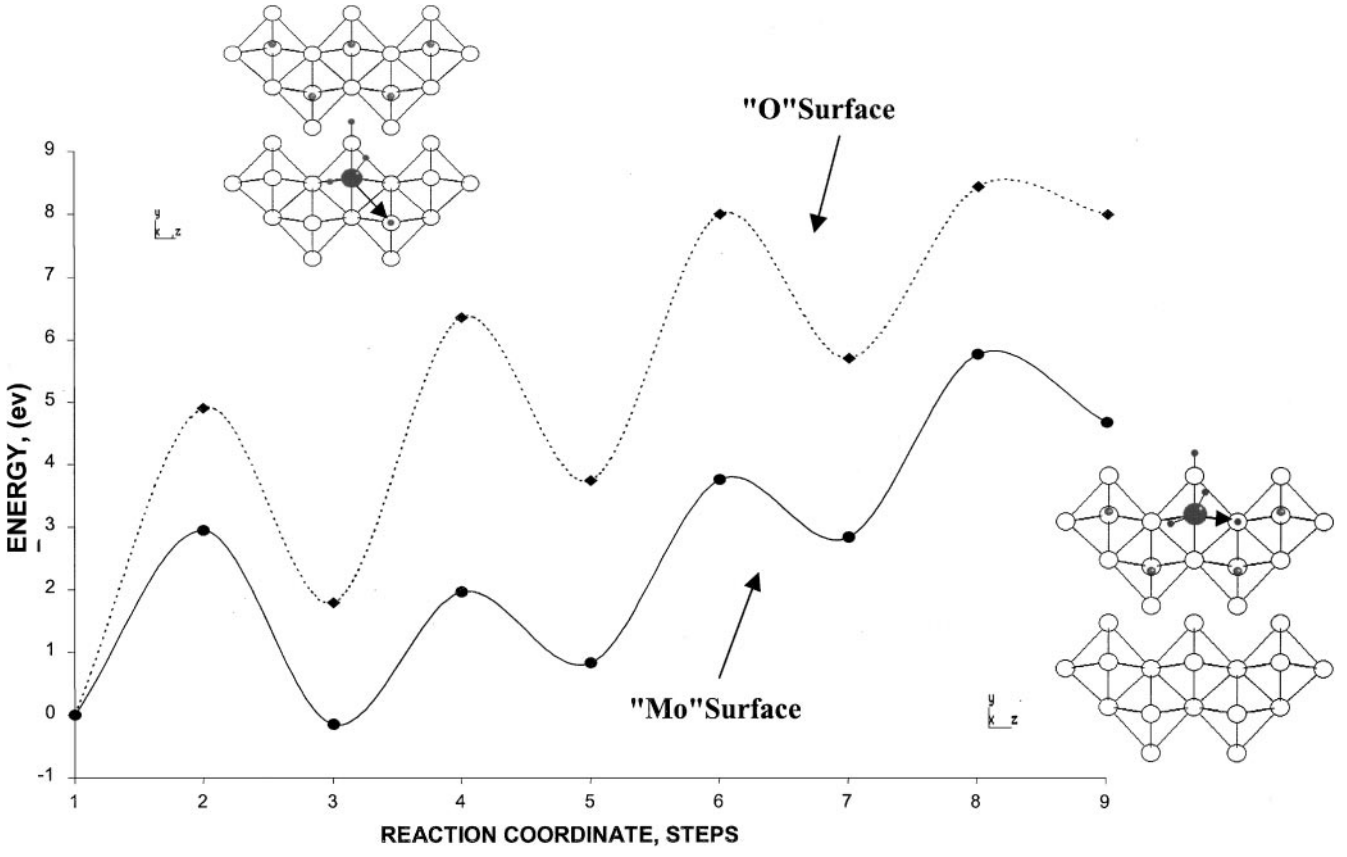

FIG. 1. Total energy vs. reaction coordinate curve for H abstraction. Top insert: Pathway for the first H abstraction from CH_3 over the layer exposing O atoms. Bottom insert: Pathway for the first H abstraction from CH_3 over the layer exposing Mo atoms. •, H; ●, O; ●, Mo; ●, C.

corresponding to the different C–H bonds are synthesized in Figs. 2 and 3. The OP(C–H) is displayed as a function of the reaction coordinate steps, where the 1, 3, 5, 7, and 9 values correspond to valleys and 2, 4, 6, and 8 to hills in adsorption energy (as labeled in Fig. 1), i.e., the presence of an activation energy, for the breaking of the first, second, third, and fourth C–H bond, respectively.

In the homolytic rupture the first C–H bond is broken just before CH_4 reaches the energy barrier (see Fig. 2), while the O–H bond is only formed once this barrier is overcome (with a OP(O–H) of ~0.8). For the next two H-atom abstractions from CH_4, in which the H–O bonds are

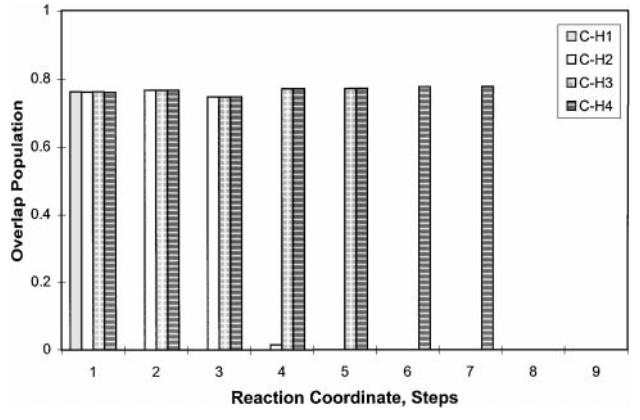

FIG. 2. C–H overlap populations over the layer exposing O atoms. The atom subindex refers to the H abstraction involucrated.

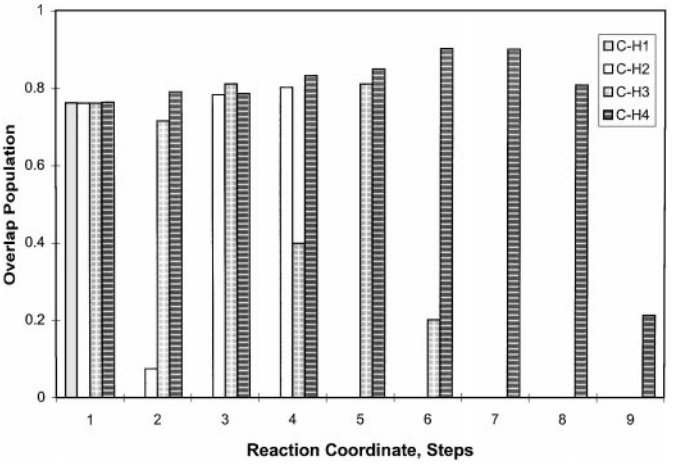

FIG. 3. C–H overlap populations over the layer exposing Mo atoms. The atom subindex refers to the H abstraction involucrated.

involved, a similar behavior can be observed; i.e., the C–H bond breakage occurs before the corresponding hydrocarbon fragment reaches the energy barrier.

During the last C–H rupture, which corresponds to total CH_4 dehydrogenation, a strong C–O bond is formed. This observation shows an opposite behavior in comparison with the nonbonding or nearly nonbonding character obtained for the C–O bonds in the preceding three H-abstraction sequences. The C atom begins to bind to the O atom with OP(C–O) = 0.27 at step 8 when the C–H bond is just broken. Finally, the C–O bond is completely formed at step 9 where OP(C–O) = 1.37. The last process leaves an oxygen vacancy on the oxide surface, resulting in a partial reduction of the catalyst. The cumulative effect of such reactions produces MoO_3 deactivation, unless a reoxidation with gaseous oxygen is provided (22, 23). Moreover, it is worth noting that the last O–H interaction is of nonbonding character, indicating the presence of one chemical species susceptible to further dissociation.

Regarding the heterolytic rupture, looking at Fig. 3 it can be observed that the first C–H bond breaks before the CH_4 surmounts the energy barrier at step 2. In addition, the first O–H bond is formed at this barrier where OP(O–H) = 0.75. This fact is accompanied with a weakening of the second C–H bond as well as the formation of a C–Mo bond with OP(C–Mo) = 0.48. Noticeably, at the end of this process, a rebuilding of the second C–H bond is observed, where OP(C–H) changes from 0.07 to 0.78. This behavior exhibited by one of the C–H bonds in CH_3 can be rationalized by considering that a significant mixing between CH_3 and the surface MoO_3 molecular orbitals is produced. The C–H bond becomes weaker because the carbon atomic orbitals are in this case coupled with both the H atomic orbitals and the surface MoO_3 molecular ones. Furthermore, this situation is also compatible with a lower activation energy barrier in comparison with that corresponding to the homolytic mechanism.

During the second H-atom abstraction, one of the involved C–H bonds shows an analogous behavior to that previously found in the first H abstraction. On the other hand, the last C–H bond to be broken remains without significant OP changes during the different partial dehydrogenations, but it decreases in the last step. The C–Mo bond becomes increasingly strong, during these abstractions, reaching OP(C–Mo) = 1.54 at step 9. However, during the final C–H rupture, the C–Mo overlap population decreases from 1.29 to 1.03, at step 8. This observation and the decrease of OP(C–H) in the last step can be explained by recalling that this process requires a spatial reorientation of the fragment (Ref. (28)).

Taking into account our previous electronic structure analysis, a comparison of the two described dehydrogenation mechanisms can be made. During the homolytic C–H bond rupture, chemical interactions between CH_x fragments and the oxide surface are of a nonbonding character. Besides, the C atom becomes strongly bonded to the surface O atom only in the last C–H bond breaking. On the other hand, during the heterolytic C–H bond scission, the C–Mo chemical interaction is of a strong and increasingly bonding character. This observation explains why the heterolytic CH_4 dehydrogenation mechanisms prove to be more favorable than the homolytic ones, making the "Mo" layer more active from a catalytic point of view.

TABLE 1

Calculated Values for CH_3 and CH_2 Interactions with the MoO_3 Cluster Surface

	"O" layer	"Mo" layer	Energy difference
Reaction energy CH_3 (eV)[a]	1.80	−0.15	1.95
Adsorption energy[b]	0	−1.54	1.54
OP C-surface atom[a]	0	0.45	
OP C-surface atom[b]	0	0.45	
Reaction energy CH_2 (eV)[a]	3.74	0.84	2.90
Adsorption energy[b]	0	−2.88	2.88
OP C-surface atom[a]	0	1.00	
OP C-surface atom[b]	0	0.79	

[a] See Fig. 1.
[b] Isolated species.

Taking the above OP analysis into account, it can be concluded that the "Mo" layer, in comparison with the "O" layer, has a special affinity for the C atom. To test this assessment invoking also energetic arguments, the adsorption energy for the isolated intermediate CH_3 and CH_2 species was calculated at the same geometric position as in the presence of abstracted H atoms (see inserts in Fig. 1). In Table 1 the corresponding results are summarized for the "O" and "Mo" layers. It can be observed that these hydrocarbon fragments have no chemical binding with the cluster "O" layer. On the other hand, they show significant energy stabilization on the "Mo" cluster layer, in agreement with the reaction energy profile of Ref. (28). The difference between the reaction energy profiles for the heterolytic and homolytic mechanisms at steps 3 and 5 are in very good agreement with the adsorption energy differences evaluated for the isolated species. The OP populations corresponding to C-surface atom interactions for the isolated fragments are also reported (see Table 1). They are very similar to the values obtained for the overall dehydrogenation process. Therefore, our approach based on the study of CH_3 and CH_2 adsorption reactions on a clean catalyst surface can be used as a reasonable and approximate model for the molybdenum oxide chemical reactivity.

The electronic structure of the free MoO_3 cluster is constituted essentially by a full-occupied band deriving from the 2*p* levels of O and a higher empty band from 4*d* and 5*s* atomic levels of Mo. In Fig. 4, the total DOS of bare

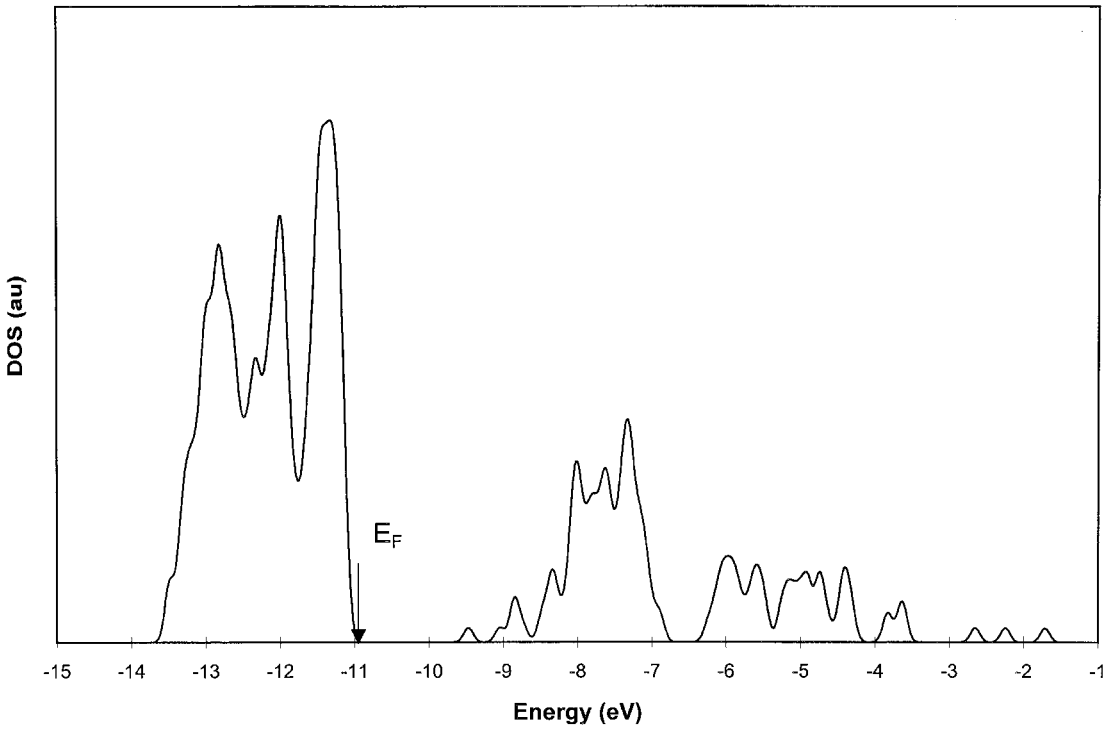

FIG. 4. Total electronic DOS of the MoO_3 cluster.

MoO_3, calculated according to Eq. [2], is presented. It reveals the typical structure of an insulator, with a band gap of 1.5 eV between the valence and conduction bands. This result is ≈40% lower than the experimental reported value of 2.8 eV obtained from X-ray photoelectron spectroscopy experiments (35). It can be considered quite reasonable, taking into account that in our semiempirical approach the parameters were not optimized to reproduce bulk properties of MoO_3 and that, on the other hand, the band gaps obtained with ab initio methods were exceedingly large in comparison with the experiment. Indeed, using the Hartree–Fock (36) or density functional theory (37) values of 16.02 and 19.87 eV were reported for the band gap, respectively.

In the following, a detailed description of the electronic structure of fragment molecular orbitals (FMO) of adsorbed CH_3 and CH_2 is performed. The electronic structure of the free CH_3 species can be described using seven valence orbitals, four of them normally occupied (38). The orbitals with symmetry $2A_1$, 1E (4-fold degenerate), and $3A_1$ (single occupied), which could hybridize with the valence levels of MoO_3, follow this sequential order in energy: $2A_1 < 1E < 3A_1$. On the other hand, for free CH_2, six valence levels, three of them normally occupied, are necessary. They are named $2A_1$, $1B_2$, and $3A_1$, in this order of energies: $2A_1 < 1B_2 < 3A_1$. Considering the symmetry with respect to an axis passing through the C atom, the $2A_1$ and $3A_1$ levels of both molecules can be classified as having σ symmetry, while the 1E and $1B_2$ levels have π symmetry (38).

The p-LDOS of 1E and $3A_1$ projections of the CH_3 fragment for the "O" and "Mo" layers are shown in Figs. 5 and 6, respectively. The results for the "O" layer are analyzed first. The 1E projections are located immediately below the bottom of the 2*p* band, while the $3A_1$ ones are placed above the top of this band (see Fig. 5). Nevertheless, they show an incipient hybridization reflecting the small OP(C–O) values mentioned above. In other words, the mean value of the molecular orbital projections are very close to the energy levels of the free CH_3. The projection of the lower $2A_1$ state shows a completely analogous behavior to that of the other two states. The integration of these p-LDOS up to the Fermi level give us the molecular orbital populations. The corresponding values are collected in Table 2.

TABLE 2

Molecular Orbital Populations

	"O" layer	"Mo" layer
	CH_3/Cluster	
Molecular orbital, $2A_1$ (σ)	2	1.90
Molecular orbital, 1E (π)	2	1.91
Molecular orbital, 1E (π')	2	1.91
Molecular orbital, $3A_1$ (σ)	1	1.64
	CH_2/Cluster	
Molecular orbital, $2A_1$ (σ)	2	1.78
Molecular orbital, $1B_2$ (π)	2	1.78
Molecular orbital, $3A_1$ (σ)	2	1.61
Molecular orbital, $1B_1$ (P)	0	0.59

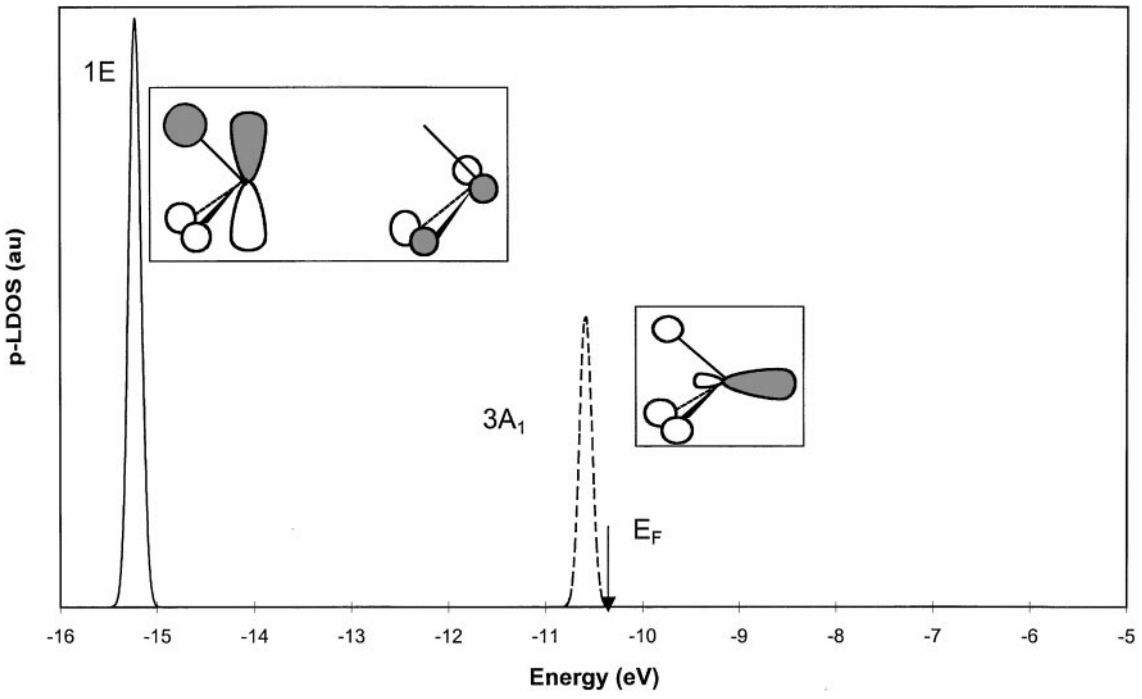

FIG. 5. CH_3 projected-LDOS over the layer exposing O atoms. ε_{1E} (free CH_3) = −15.23 eV; ε_{3A_1} (free CH_3) = −10.59 eV.

Note that the orbital population is basically that of the free molecule.

Regarding the results for the "Mo" layer in Fig. 6, they show that while the 1E projections are not significantly hybridized, the $3A_1$ ones show a significant coupling with the 2*p* band of MoO_3, with a broadening of nearly 3 eV below the Fermi level. This observation is in accord with the significant OP(C–Mo) values referred to above. Moreover, looking at the corresponding molecular orbital populations in Table 2, it can be observed that this hybridization is

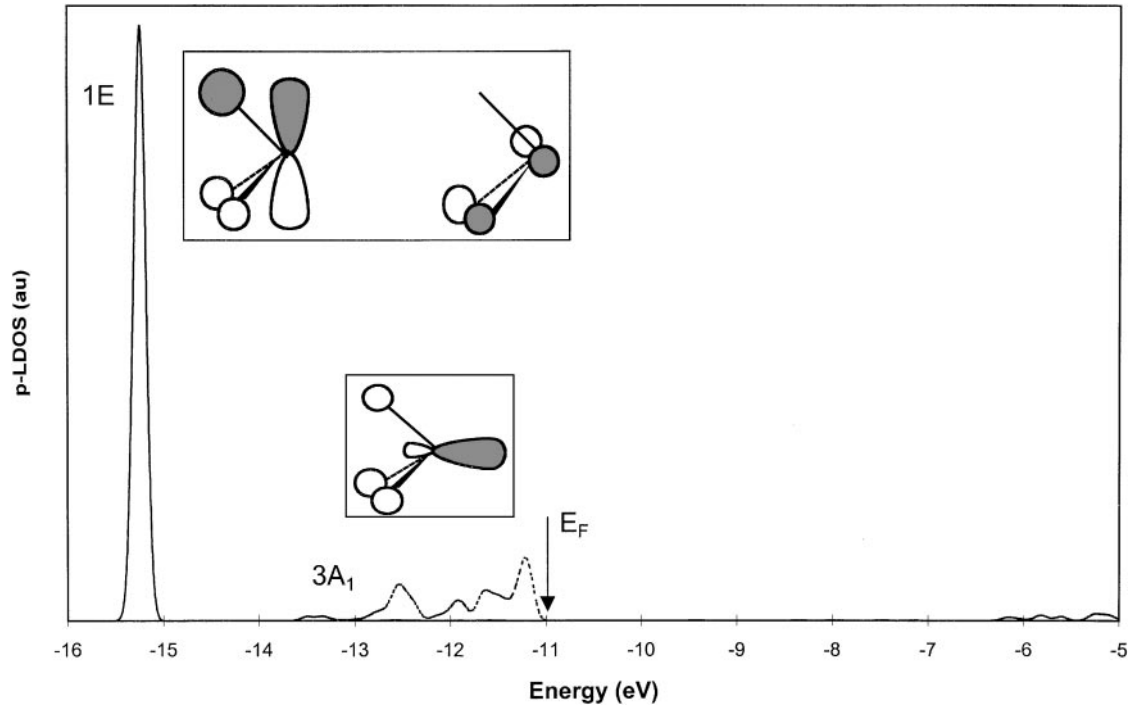

FIG. 6. CH_3 projected-LDOS over the layer exposing Mo atoms. ε_{1E} (free CH_3) = −15.23 eV; ε_{3A_1} (free CH_3) = −10.59 eV.

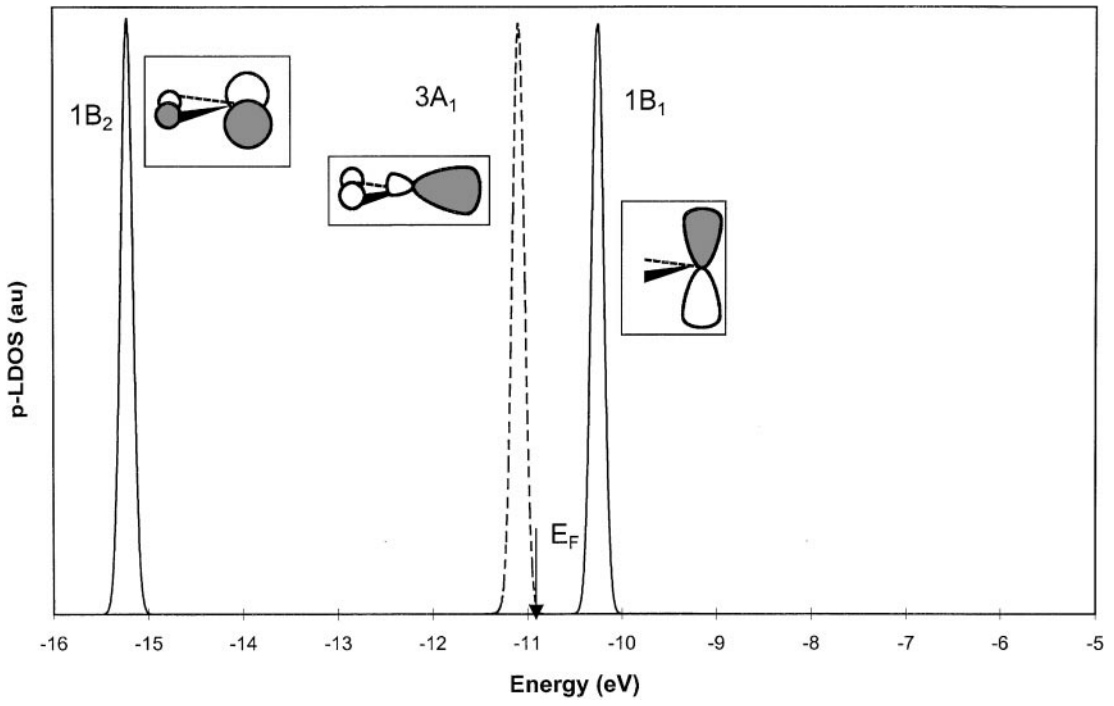

FIG. 7. CH_2 projected-LDOS over the layer exposing O atoms. ε_{1B_2} (free CH_2) = −15.40 eV; ε_{3A_1} (free CH_2) = −10.98 eV; ε_{1B_1} (free CH_2) = −10.26 eV.

accompanied by small electronic donations (of ≈0.1 e^-) from the lower energy levels (including the $2A_1$ orbitals) to the CH_3 fragment and a larger back-donation (of ≈0.64 e^-) to the $3A_1$ state.

The p-LDOS of $1B_2$, $3A_1$, and $1B_1$ projections of the CH_2 fragment on the "O" and "Mo" layers are exhibited in Figs. 7 and 8, respectively. The "O" layer is considered first. Note that, in this case, the three molecular orbitals have only a

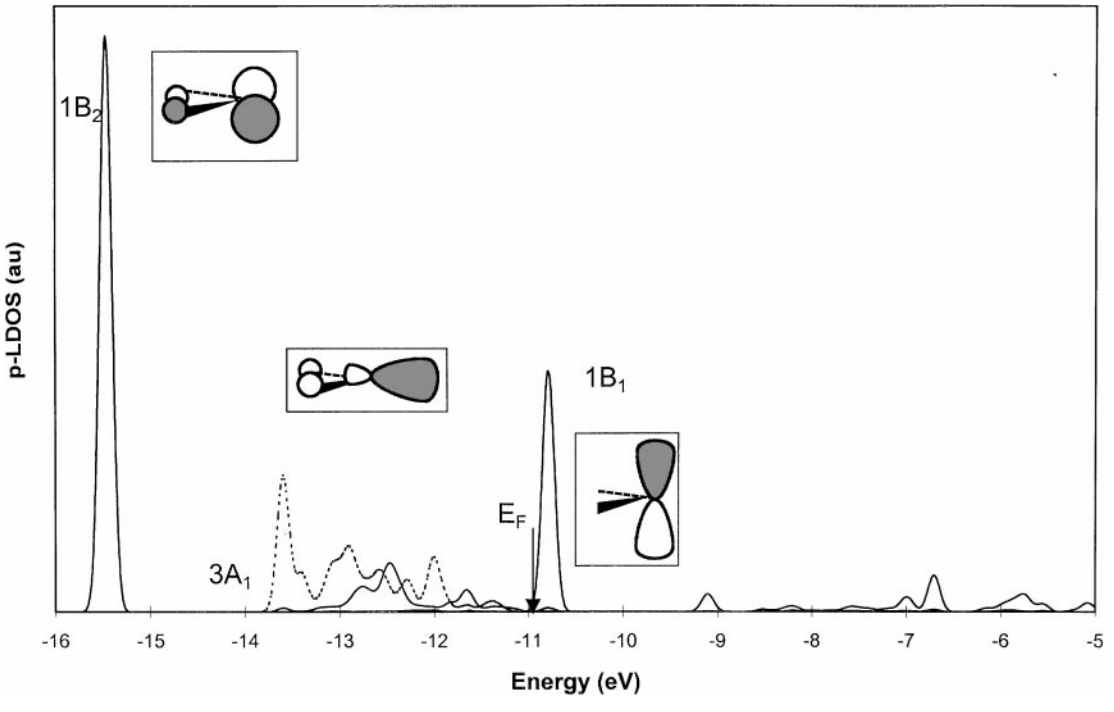

FIG. 8. CH_2 projected-LDOS over the layer exposing Mo atoms. ε_{1B_2} (free CH_2) = −15.40 eV; ε_{3A_1} (free CH_2) = −10.98 eV; ε_{1B_1} (free CH_2) = −10.26 eV.

small degree of hybridization, in direct relation to the small OP(C–O) values. Moreover, the molecular orbital populations of Table 2 indicate that the occupations for each of these states correlate with those of a nonperturbed free CH_2 species. This observation is also valid for the lower $2A_1$ orbital. On the other hand, on the "Mo" layer, while the $1B_2$ projections are significantly localized, the $3A_1$ and $1B_1$ projections become hybridized to a large extent. The $3A_1$ levels mix strongly with the 2*p* band of MoO_3, showing broadening near 3 eV below the Fermi level and the $1B_1$ levels also interact extensively with the 4*d* band, with an extended broadening above the band gap (see Fig. 8). However, the last electronic states are not occupied and are not taken into account in the orbital population of $1B_1$ projections. All these results are summarized in Table 2. Indeed, while the $2A_1$ and $1B_2$ states become somewhat depopulated (by $\approx$0.2 e^-), the $3A_1$ one depopulates more noticeably (by $\approx$0.4 e^-) and the usually empty $1B_1$ state populates to a large extent (by $\approx$0.6 e^-) (see Table 2).

An interesting parallelism can be made between the behavior of CH_3 and CH_2. The electronic structure of fragments residing on the "O" layer correlates, in both cases, with that of the free species. On the other hand, on the "Mo" layer, an important mixing results between the 2*p* band of MoO_3 and the $3A_1$ molecular orbital of CH_3 and CH_2. These kinds of orbitals have a particular symmetry, where a lobe of the $2p_z$ orbital of carbon is directed in opposition to the dihedral angle of CH_3 or the planar angle of CH_2 (see the molecular orbital schemes inserted in Figs. 6 and 8), allowing a significant overlap with the 2*p* orbitals of MoO_3 to be achieved.

4. CONCLUSIONS

In the present work an analysis of the electronic structure of intermediates in CH_4 dehydrogenation on MoO_3(100) was accomplished for two surface regions: the so-called "O" and "Mo" layers. A careful examination of the overlap population between the C and the substrate atoms was performed. In the homolytic mechanism each C–H bond breakage occurs before the corresponding hydrocarbon fragment reaches the energy barrier and the O–H is formed after surmounting this barrier. A strong C–O chemical bond is established as a consequence of the last H abstraction. On the other hand in the heterolytic mechanism the C–H breaking is accompanied by a temporary weakening of a second C–H bond and the formation of an increasingly strong C–Mo bond. In the last H abstraction of the methane decomposition the C–H bond is broken only in the final step, as a consequence of the spatial reorientation of the C–H species.

The analysis of p-LDOS was restricted to the most relevant molecular orbitals of CH_3 and CH_2. Calculations show that a significant chemical interaction is only present on the "Mo" layer. This process is accompanied by a notable hybridization of the molecular orbitals around the Fermi level of MoO_3. On the other hand, the C-surface interaction is mainly nonbonding in the case of the exposed "O" layer. All these results help us to a better understanding of the CH_4 dehydrogenation on molybdenum oxide surfaces, in terms of electronic structure arguments.

ACKNOWLEDGMENTS

This work is partially supported by Fundación Antorchas, CONICET (Argentina), ANPCYT, (PICT 12-03576) and a direct research grant from Departamento de Física-UNS. A. Juan and N. Castellani are members of CONICET.

REFERENCES

1. Hutchings, G. J., Scurrell, M. S., and Woodhouse, J. R., *Chem. Soc. Rev.* **18**, 251 (1989).
2. Lee, J. S., and Oyama, S. T., *Catal. Rev.-Sci. Eng.* **30**, 249 (1989).
3. Kalenik, Z., and Wolf, E. E., *J. Catal.* **10**, 180 (1993).
4. Lunsford, J. H., *Catal. Today* **6**, 235 (1990).
5. Sokolovskii, V. D., and Mamedov, E. A., *Catal. Today* **14**, 331 (1992).
6. Burch, R., and Hayes, M. J., *J. Mol. Catal. A* **100**, 13 (1995).
7. Sokolosvskii, V. D., Aliev, G. M., Buyesvskaya, O. V., and Davydov, A. A., *Catal. Today* **4**, 293 (1989).
8. Sokolosvskii, V. D., Buyevskaya, O. V., Aliev, S. M., and Davydov, A. A., *in* "New Developments in Selective Oxidation" (G. Centi and F. Trifiro, Eds.). Elsevier, Amsterdam, 1990.
9. Ito, T., and Lunsford, J. H., *Nature* **314**, 721 (1985).
10. Rahmouni, A., and Barbier, C., *J. Mol. Struct.* **330**, 359 (1995).
11. Tatibouet, M. T., and Germain, J. E., *J. Catal.* **76**, 238 (1982).
12. Ziólkowski, J., *J. Catal.* **80**, 263 (1983).
13. Liu, H. F., Liu, R. S., Liew, D. J., Johnson, R. E., and Lunsford, J. H., *J. Am. Chem. Soc.* **106**, 4117 (1984).
14. Khan, M. M., and Somorjai, G. A., *J. Catal.* **91**, 263 (1985).
15. Spencer, N. D., Pereira, C. J., and Grasselli, R. K., *J. Catal.* **126**, 546 (1990).
16. Smith, M. R., and Ozkan, U. S., *J. Catal.* **141**, 124 (1993).
17. Smith, M. R., and Ozkan, U. S., *J. Catal.* **142**, 226 (1993).
18. Pack, S., Rosynek, M. P., and Lunsford, J. H., *J. Phys. Chem.* **98**, 11786 (1994).
19. Halasz, J., Brenner, A., and Shelef, M., *Catal. Lett.* **16**, 311 (1992).
20. Halasz, J., Brenner, A., and Shelef, M., *Catal. Lett.* **18**, 289 (1993).
21. Konopny, L., Juan, A., and Damiani, D. E., *Appl. Catal. B* **15**, 115 (1998).
22. Bielanski, A., and Haber, J., *in* "Oxygen in Catalysis," Vol. 43. M. Dekker, New York, 1990.
23. Tatibouet, J. M., *Appl. Catal. A* **148**, 213 (1997).
24. Sambeth, J., Juan, A., Gambaro, L., and Thomas, H., *J. Mol. Catal.* **118**, 283 (1997).
25. Rahmouni, A., and Barbier, C., *J. Mol. Struct.* **330**, 359 (1995).
26. Weber, R., *J. Phys. Chem.* **98**, 2999 (1994).
27. Mehandru, S. P., Anderson, A. B., Brazdil, J. F., and Grasselli, R. K., *J. Phys. Chem.* **91**, 2930 (1987).
28. Irigoyen, B., Castellani, N., and Juan, A., *J. Mol. Catal.* **129**, 297 (1998).
29. Anderson, A. B., *J. Chem. Phys.* **60**, 2477 (1974).
30. Anderson, A. B., and Hoffmann, R., *J. Chem. Phys.* **60**, 4271 (1974).
31. Anderson, A. B., *J. Chem. Phys.* **62**, 1187 (1975).
32. Hoffmann, R., *J. Chem. Phys.* **39**, 1397 (1963).
33. Mülliken, R. S., *J. Chem. Phys.* **23**, 1833 (1955).
34. Rivail, J. L., *in* "Eléments de Chimie Quantique." Inter. Editions, Editions du CNRS, Paris, 1990.
35. Henrich, V. E., *Rep. Prog. Phys.* **48**, 1481 (1985).
36. Papakondylis, A., and Sautet, P., *J. Phys. Chem.* **100**, 10681 (1996).
37. Corá, F., Patel, A., Harrison, N. M., Roetti, C., and Catlow, C. R. A., *J. Mater. Chem.* **7**, 959 (1997).
38. Jorgensen, W. L., and Salem, L., *in* "The Organic Chemist's Book of Orbitals." Academic Press, New York, London, 1973.